MISTRA SWECIA
CLIMATE, IMPACTS & ADAPTATION

Mistra-SWECIA Working Paper

No 3

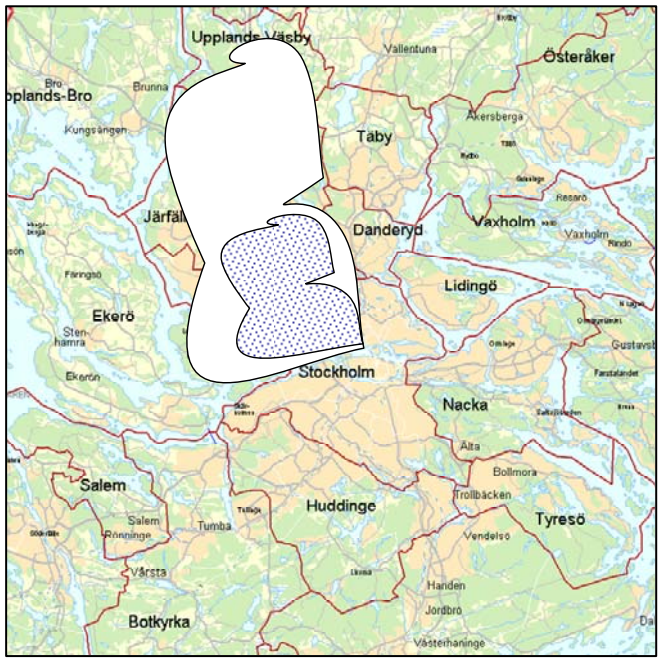

Downscaling extreme RCA3-precipitation for urban hydrological applications

Jonas Olsson and Ulrika Willén
Research Department, Swedish Meteorological and Hydrological Institute

FUNDED BY MISTRA

Downscaling extreme RCA3-precipitation for urban hydrological applications

Jonas Olsson and Ulrika Willén
Research Department, Swedish Meteorological and Hydrological Institute

May 2010

Contents

Acknowledgements

Erik Kjellström and Anders Ullerstig provided most of the RCA3 data used in this study.

Summary

In this report, the prospect of simulating extreme local (i.e. sub-gridscale) short-term (30-min) precipitation from the RCA3 regional climate model is investigated. A simple stochastic downscaling scheme based on cloudiness and precipitation components is formulated and evaluated.

A comparison of ERA40-driven RCA3-simulations with observations shows that the annual cycle of mean monthly total precipitation from RCA3 agrees well with observations, although there is some slight overestimation. The frequency is, however, overestimated, especially of large-scale (resolved) precipitation. Also the mean monthly RCA3 cloud cover agrees well with observations. In future climate projections, no clear changes in the cloud cover are found. Large-scale and convective precipitation all increase gradually by some 20% by the period of 2071-2100. Total and extreme large-scale precipitation increases mainly in winter; convective precipitation in summer.

With the stochastic downscaling scheme is able to simulate point precipitation time series which satisfactorily reproduce observed extreme statistics. The downscaled series indicate a 5-10% increase in short-term extreme intensities in the period of 2011-2040 and a 10-20% increase in the period of 2071-2100. This is 5-10% more than the increase estimated from RCA3 gridbox data. Using more detailed cloud variables than 'total clouds' and 'high clouds' did not improve performance of the downscaling scheme.

1. Introduction

Urban hydrological modelling requires precipitation data at a very high resolution, in both time and space. In time, durations down to 5-10 minutes need to be considered. In space, generally observations from a single gauge (or a few gauges within a very limited area) are used. The precipitation input may be either continuous time series with observed historical sequences or idealised design storms. In the latter case, precipitation intensity is estimated from so-called Intensity-Duration-Frequency (IDF) curves.

The high resolutions required are problematic with respect to climate change assessment, as they are not matched by the resolutions used in Global Climate Models (GCMs) or either Regional Climate Models (RCMs). The calculation time step used in the latter (30 min, sometimes shorter) is rather close to the required temporal resolution, but the still relatively coarse spatial grid used in the calculations (typically 50×50 km, sometimes finer) makes RCM output unsuitable for direct application in urban hydrological climate change assessment.

The properties of short-term precipitation as observed in a single gauge and as averaged over a few thousand km², respectively, are very different. The most important difference concerns the extremes. The observed extremes can be very localised whereas a model gridbox represents an average of surface types and heights. Thus, the model extremes are expected to differ. Further, since the observed extremes occur over very short time periods, often shorter than the model time step, short term atmospheric fluctuations will not be fully captured by the model. In Sweden, local extremes are practically always generated in summer by localised short-term convective events. In the models, depending on the resolution and the convective parameterisation, these convective events can occur either on the resolved model grid box scale or on sub-grid scale. Thus, analyses of RCM extremes (and their changes) at the gridbox scale may not reflect the properties of local extremes.

The objective of the study is to assess the possibility to stochastically downscale extreme precipitation from the RCM grid scale to local scale. The main assumption behind the approach is that additional RCM variables, mainly precipitation type and cloud cover, can be used to rescale gridbox average precipitation to local precipitation. By assigning a probability that this local precipitation occurs in a specific point inside the gridbox, realisations of point value time series may be stochastically generated. The overall idea is to formulate such a stochastic scheme, calibrate it to reproduce observed statistical properties for the present climate, and then apply the calibrated scheme to estimate future point precipitation statistics.

2. Study area and data

In this chapter, the different types of data used in the analysis are described and evaluated.

2.1. Local precipitation observations

Daily precipitation volumes (resolution 0.1 mm) during the period 1980-2007 were extracted from SMHI-station 9821 (denoted SMHI in the following), which is located at the Royal Institute of Technology campus in the northern part of central Stockholm.

Short-term data from a tipping-bucket gauge on Torsgatan, central Stockholm, are available for the period 1984-2004 (except 1994) (denoted TB in the following). This series is mainly used for analyses of extremes and therefore minor rainfall events have been removed; thus the series is not suitable for assessments of e.g. rainfall totals. The maximum attainable time resolution of the gauge is 5-10 seconds, but in practice the useful resolution is 1-2 minutes. The volume resolution is 0.1 mm. For most of the analyses performed in this study, the time series were converted from the original time resolution into 30-min accumulations.

In urban hydrology and design, the properties of short-term rainfall extremes are generally compactly described in the form of Intensity-Duration-Frequency (IDF) curves, based on extracted rainfall maxima for different durations. In such a diagram, the x-axis represents duration, the y-axis mean intensity during this duration, and the resulting curve a certain return period. In engineering practice, IDF curves are used to determine which rainfall intensity a storm water sewer must be able to handle. In Sweden a 10-year return period is design standard, with duration depending on the catchment size, often 30 min or 1 hr.

Hernebring (2006) has performed Intensity-Duration-Frequency (IDF) analysis of short-term data from 15 stations all over Sweden, including the TB data used here, and he proposed the following general relationship (IDF curve)

$$I = e^{(k_{11}+k_{31}/D)} * R^{(k_{12}+k_{32}/D)} * D^{(k_{21}+k_{22}*\ln(R))} \quad (1)$$

where I denotes intensity, D duration, R return period and k location-specific constants. The relationship was found valid between durations of 5 min and 24 hrs. For Stockholm the constants were found to be k_{11}=6.24, k_{12}=0.53, k_{21}=-0.69, k_{22}=-0.031, k_{31}=-1.77 and k_{32}=-0.61. Hernebring (2006) does not show the agreement between observed intensities and the fit of (1) for Stockholm, but in total over all stations considered the fit appears very accurate.

2.2. Climate model description and data

In this subsection we briefly describe the cloud and precipitation parameterizations in the regional climate model RCA3 and the data from the climate simulations. For a full model description we refer to Jones et. al. (2004) and Kjellström et. al. (2005).

2.2.1 Clouds and precipitation in RCA3

Clouds and precipitation in climate models are difficult to predict since most clouds are produced by condensation processes that take place on spatial scales much smaller than the size of a model gridbox, e.g. clouds produced by cumulus convection, boundary layer turbulence, gravity waves or orographic lifting. These clouds have to be parameterised as functions of the prognostic variables explicitly resolved by the model, without loosing the information about the physical processes that occur on the subgrid scale and that are responsible for these clouds (Bony and Emanuel, 2001). Cloud fraction parameterizations can be classified into two main types, diagnostic schemes and statistical schemes. The statistical schemes use specified probability distribution functions (PDFs) to represent subgrid scale variability of total water (water vapour, cloud water and ice). The cloud fraction can be determined from the supersaturated part of the PDF. The shape and width of the distributions are determined from observations or high resolution cloud resolving models.

RCA3 cloud parameterization belongs to the diagnostic group and has cloud processes separated into resolved clouds (large- and mesoscale) and sub-grid scale (convective) clouds. Resolved clouds including e.g. frontal clouds, are described using the scheme of Rasch and Kristjansson (1998) which is based upon the work of Sundqvist (1988) with a prognostic equation for the total cloud condensate (cloud water and ice). Convective clouds are described using the approach of Kain and Fritsch (1990). In this scheme only the active convective updrafts and downdrafts are parameterized and the mesoscale portion of any convective system, such as convective anvils, are assumed to be resolved by the model grid system and will contribute to the resolved part of the parameterization. Detrained convective water and ice acts as a source term for the resolved condensation resulting in a tight coupling between convection and the resolved condensation and clouds.

The diagnosis of the cloud fraction in a grid square follows the ideas of Slingo (1987). Various modifications of the calculations of resolved and sub-grid scale clouds have been introduced in RCA. The large scale cloud fraction is diagnosed based on grid box mean relative humidity and fractional clouds and condensation can form before a model grid box is saturated using a predefined threshold relative humidity. An active convective cloud fraction is also calculated for the parameterized convective updrafts using the diagnostic approach of Xu and Krueger (1991).

Precipitation is calculated for the resolved and sub-grid scale clouds separately. In this report we will refer to them as large scale and convective precipitation bearing in mind that the RCA3 resolved precipitation also contains convective parts. Brown (1979) estimates that up to 40% of the precipitation reaching the ground in a typical convective system originates from the mesoscale cloud system

2.2.2 RCA3 data

The regional climate model data come from four RCA3 simulations. For present day climate, 1980-2007, we used boundary fields from ERA40 (1980-mid 2002) and from operational ECMWF analyses (mid 2002-2007). RCA3 was also run with boundary fields from two transient ECHAM4-scenarios (A2, B2) and one ECHAM5-scenario (A1B). The transient scenario runs

cover the entire period 1961-2100, but four 30-year periods have been defined for this study: 1971-2000 (reference period; REF), 2011-2040 (future climate 1; FC1), 2041-2070 (FC2) and 2071-2100 (FC3). All runs were performed over Europe at 50km horizontal resolution with 102*111 gridpoints and 24 vertical levels.

As the investigation is focused on Stockholm, data from five gridboxes, each representing an area of 50×50 km, in the region have been extracted and analysed: the one centred over central Stockholm, and the one in each quarter (N, E, S, W). The variables that have been used are:

- Total precipitation, TP (time step: 30 min)
- Large and meso-scale precipitation (resolved), LP (3 hr)
- Convective precipitation (sub-grid scale), CP (3 hr)
- Total cloud cover: total, TC (3 hr)
- High clouds, HC (6 hr)

For all variables the time resolution is the highest available. The total cloud cover as viewed from the surface is in RCA3 calculated assuming maximum-random overlap, which is supported by observations (e.g. Willén et al., 2005). This means that adjacent cloud fractions in the vertical column (e.g. convective tower cloud extending over several model levels) are vertically stacked, i.e. in maximum overlap, while if the cloud fractions are separated by clear air (e.g. a cirrus cloud above low level shallow cumulus) they are assumed to be in random overlap. High clouds in RCA3 are defined as the maximum cloud fraction above 450hPa, medium clouds (the maximum cloud fraction in the pressure range 800 to 450hpa) and low clouds (the maximum cloud fraction below 800hPa).

3. Characterisation and evaluation of climate model data

In this chapter the climate model output in terms of precipitation and cloud cover are assessed by (1) comparing historical simulations with observations and (2) characterising future changes.

3.1. Precipitation

3.1.1. Historical RCA3 simulation (ERA40)

In this section, the short-term precipitation outputs from the RCA3 model with the ERA40-analysis at the boundaries (time period 1981-2000) are characterised. Also, some comparison is made with the local precipitation observations from Stockholm described in Section 2.1. The RCA values given represent averages over the five gridboxes used (Section 2.2), i.e. the calculations were first made for each gridbox time series, after which descriptive statistics (Table 1) were averaged over all gridboxes.

Table 1 shows that out of the mean 0.037 mm/30 min in the RCA total precipitation (TP) output, corresponding to 640 mm/yr, 75% is related to large-scale precipitation (LP) and 25% to convective precipitation (CP). As the LP percentage wet, i.e. the percentage of time with a non-zero precipitation, is 30.2% and the CP fraction is 2.7%, when precipitation actually falls the intensity is on average almost four times higher for CP. Also the maximum value is higher for CP. The most notable differences between summer and the entire year are higher mean values and wet fraction of CP, resulting in higher mean values of also TP.

Table 1 Some descriptive statistics of precipitation in RCA3/ERA40 and in the observations. Values without parentheses are calculated from the entire time series whereas values in parentheses are for summer (June-August).

	Mean (mm/30 min)	Percentage wet (%)	Mean wet (mm/30 min)	Max (mm/30 min)
RCA LP	0.027 (0.025)	30.2 (27.3)	0.091 (0.091)	2.16 (1.94)
RCA CP	0.009 (0.022)	2.7 (4.6)	0.335 (0.470)	2.81 (2.81)
RCA TP	0.037 (0.047)	32.2 (30.6)	0.114 (0.152)	2.81 (2.81)
Gauge SMHI	0.032 (0.041)	n.a.	n.a.	n.a.
Gauge TB	n.a.	n.a.	n.a.	29.4 (29.4)

Most of the RCA statistics in Table 1 can not be meaningfully compared with observations, as the TB series does not contain small events and the SMHI series has a different time resolution. Two comparisons are nevertheless made. One shows that the observed mean intensity is 0.032 mm/30 min, corresponding to 552 mm/yr, indicating that RCA3 overestimates total precipitation by some 15% (with no difference between summer and the entire year). The other comparison shows that the maximum observed 30-min point intensity is more than 10 times higher than the maximum model value. However, the maximum point observation 29.4 mm/30 min is very extreme; the second through fifth highest values are all around 14 mm/30 min, which may be a more representative maximum intensity.

When comparing maximum intensities, one aspect is the impact of spatial averaging and the resulting difference between gridded data with single point observations. Several attempts to estimate reduction factors describing the impact of spatial averaging have been made. In NERC (1975), the recommended reduction for a duration of 30 min and an area of 3000 km^2 is 0.41. A point value of 14 mm would thus correspond to 5.7 mm for an area of the size of the RCA3 grid, i.e. approximately twice the simulated value of 2.8 (see further discussion in Olsson et al., 2009). Generally, the reduction decreases with increasing time scale. For example, Haylock et. al. 2008 obtained a median reduction factor of 0.66 for daily precipitation extremes.

Another aspect concerns limitations in the climate model. We expect the model extremes to be less than the observed extremes due to the limited spatial and time resolution, mismatch in time and space (the model dynamical systems might be slightly shifted which has a large impact on the specific location) and due to shortcomings of the parameterisations. Heavy rainfall events are largely affected by the local scale and therefore we do not expect a model at 50 km (or even 10 km) resolution to capture the highest events. The model surface and orography characteristics are smoother and can differ substantially from the values at a measuring site. Furthermore, the most intense observed values occur at time intervals shorter than 30 minutes, whereas the model can only resolve atmospheric phenomena on time scales larger than the model time step, which is 30 minutes.

Despite the fact that we can list a number of possible reasons for differences between point observations and model data, the reduction factor relating a certain model's extremes to point extremes is unknown. The proposed method in section 4 is an attempt to overcome the unknown reduction factor so that we can use extremes from the model for estimating changes also in point extremes.

Figure 1 shows that the annual cycle of precipitation in the RCA3 model is in good agreement with that of the SMHI gauge, with least precipitation in spring and most in summer. The large-scale fraction is relatively stable in winter, spring and summer, but significantly higher in autumn. This is possibly a reflection a higher frequency of cyclones in this season. The contribution from active convection is significant only in summer when the land surface gets unevenly heated and nimbostratus clouds of large vertical extent can build up resulting in large precipitation amounts.

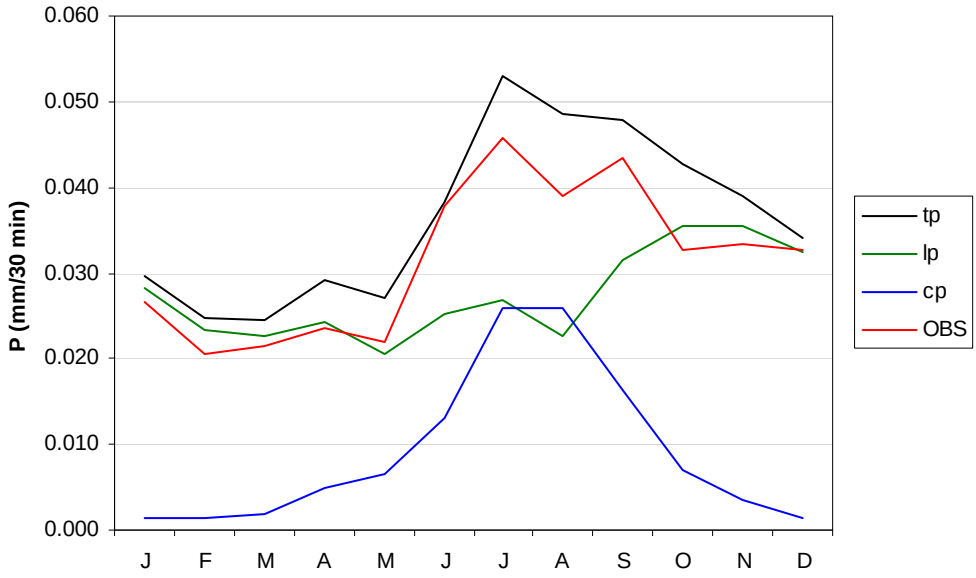

Figure 1 Annual cycle of precipitation amounts in RCA3/ERA40 (TP, LP, CP) and SMHI gauge (OBS).

As discussed in connection with Table 1, extreme precipitation intensities at a point are several times higher than those in a spatial average over 2500 km². This difference may be further assessed through IDF curves spanning different durations and respesenting different return period, as shown in Figure 2.

At *R*=15 years, and at the shortest duration 30 min the, difference between the observed (TB) and simulated (RCA3) intensity corresponds to a factor 10, in line with Table 1. Moving towards longer durations, however, the difference decreses and at 1 day the curves nearly converge. Convergence means that the point precipitation and the spatially averaged precipitation are identical, i.e. approximately the same precipitation falls everywhere inside the grid box. This in turn implies that the rainfall field produced by the type of synoptic or convective systems that generate 1-day extremes are of at least the same spatial extension as the model grid boxes. On the other hand, the rainfall systems generating short-term (sub-hourly) point extremes are mainly localised convective systems too small to produce significant spatial averages.

The curves representing shorter return periods are in principle similar to the 15-year curve (Figure 2). However, whereas the observed TB intensities substantially decrease with decreasing return period, the simulated RCA3 intensities decrease only slightly. Thus the highest spatially averaged RCA3 intensities are rather similar, whereas the observed point precipitation extremes are more variable.

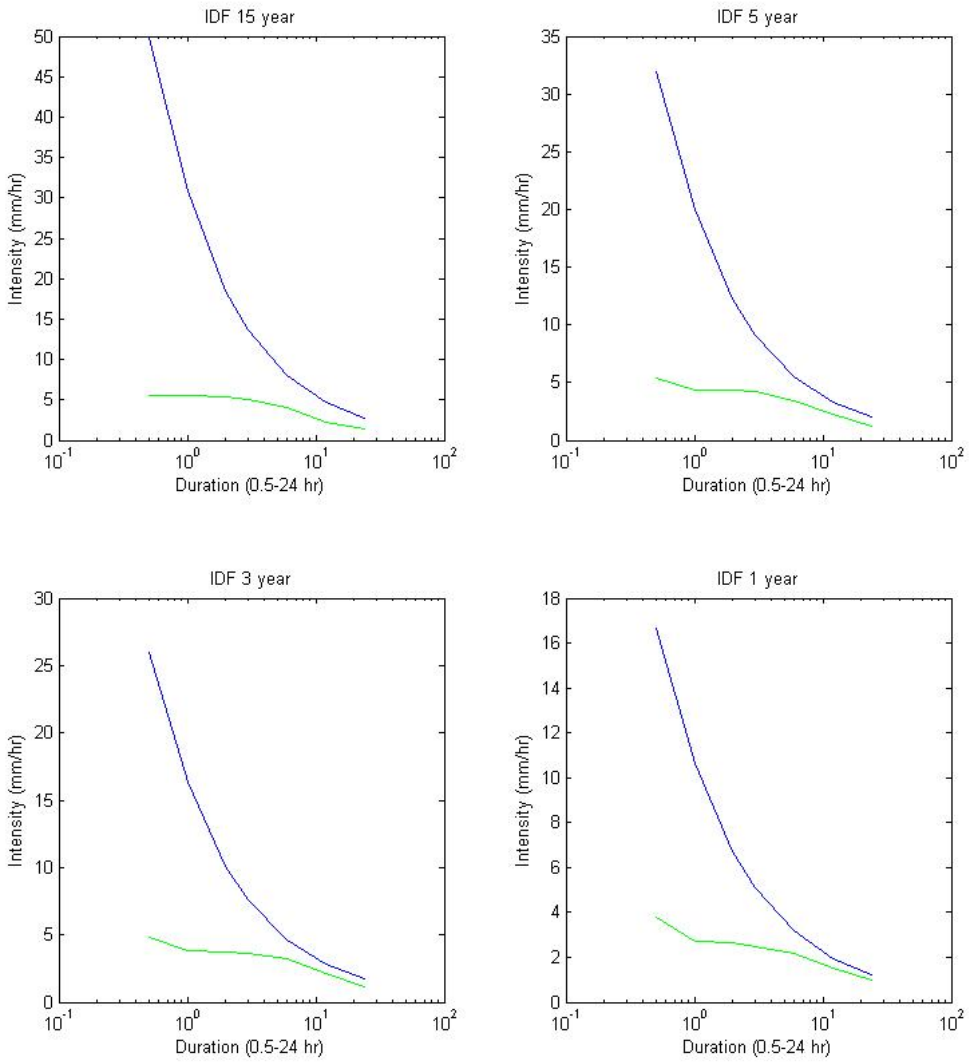

Figure 2 IDF curves representing TB observations (equation (1); blue) and RCA3/ERA40 gridbox output (green) for return periods 15, 5, 3 and 1 year.

An important aspect of the extremes and high values besides their magnitude is the seasonal variation of their occurrence. This property was investigated using the 100 highest values in the data sets. Figure 3 shows that the vast majority of observed high intensities occur in summer, with a peak in July. The RCA3 data rather well reproduces thus pattern, with some shift from spring/early summer to late summer/autumn.

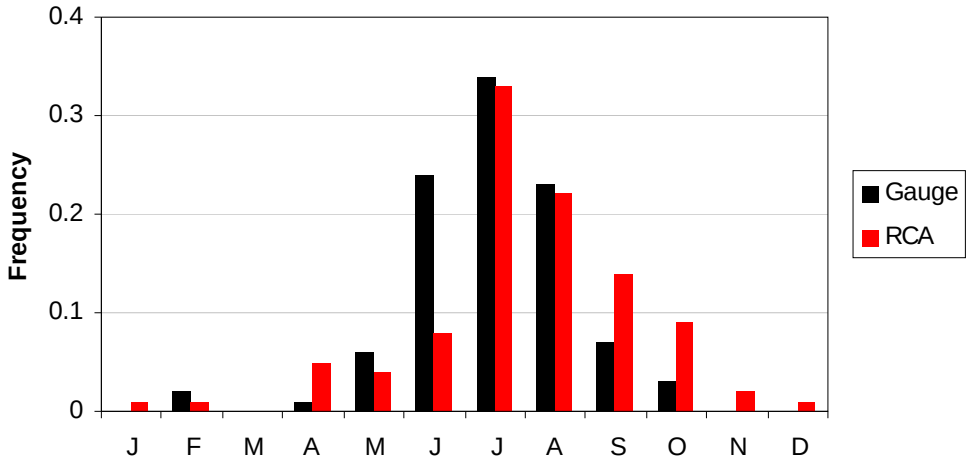

Figure 3 Monthly frequencies of extremes in the TB observations (gauge) and RCA3/ERA40 gridbox data (RCA).

A closer look at the RCA3 extremes shows that they are generally related to large-scale (resolved) precipitation, in 65% of the cases. As mentioned in section 2.2.1 the resolved precipitation also contains the meso-scale part of the convective systems. There is no clear information on this for the present observations, but the general belief is that convection is the dominant mechanism (e.g. Hernebring, 2006). This is supported by the fact that the events containing the maximum intensities are generally short, around 3 hours, and with a distinct peak. The RCA extreme events are longer, around 20 hours, and with much less intra-event variability. The short term intensity values in the IDF curves from RCA are peaks from longer duration events. It appears that the model underestimates the intense extremes in the active part of the convection, i.e. CP.

3.1.2. Future changes

In this section future changes in the Stockholm precipitation are characterised, as simulated in the three ECHAM/RCA-scenarios (Section 2.2). Figure 4 shows the precipitation for the reference period (1971-2000) and the simulated future precipitation in the B2 scenario for three 30 year periods, FC1 (2011-2040), FC2 (2041-2070) and FC3 (2071-2100). It may be noted that scenario B2 simulates slightly more precipitation in the reference period than the ERA40-driven run; the amounts being 0.041 and 0.037 mm/30 min, respectively. There is a rather constant increase of all categories. The change from REF (1971-2000) to FC3 (2071-2100) is 16% for TP, 15% for LP and 26% for CP. The A2 and A1B scenarios show overall similar tendencies.

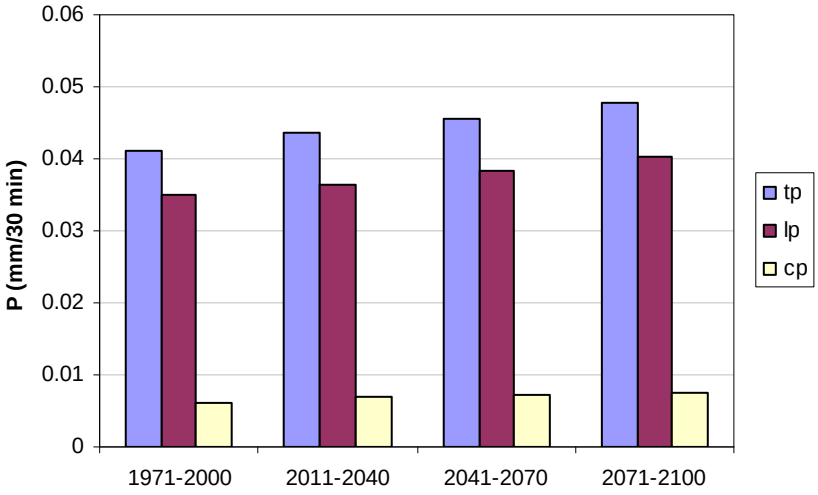

Figure 4 Mean precipitation during the 30-year periods (scenario B2).

Figure 5 illustrates how the simulated future changes vary with season. Concerning LP, most of the increase happens in winter. The change until the last period, FC3, is approximately 0.01 mm/30 min, which corresponds to 15 mm/month. During the summer half-year no clear increase can be seen. Also CP seems to increase somewhat in winter, but larger increases are indicated in summer and autumn. It may be noted that the increase in CP in some parts of summer and autumn is larger for FC2 than FC3.

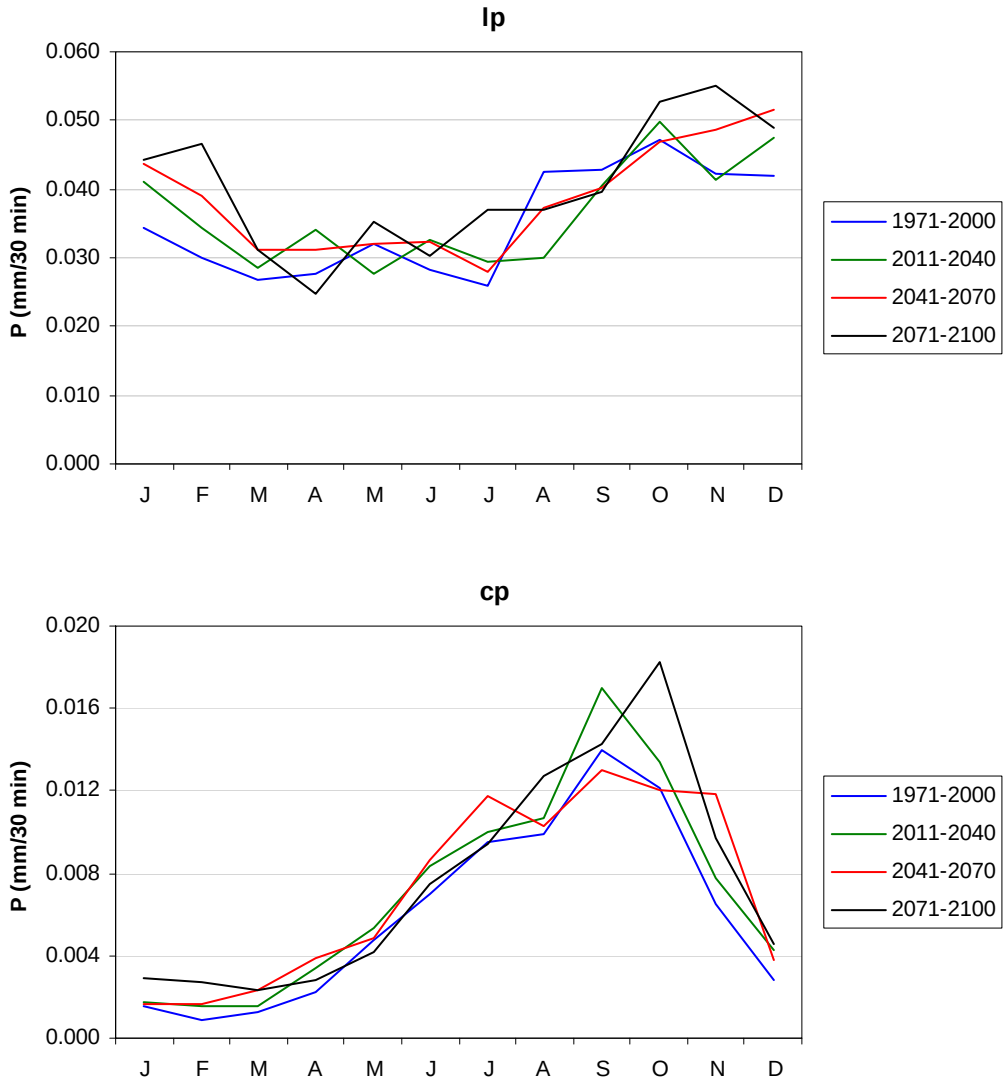

Figure 5 Monthly mean large-scale (LP; top) and convective (cp; bottom) precipitation during the 30-year periods (scenario B2).

Simulated changes in extreme precipitation were investigated by considering the 97.5th percentile of the intensity distribution. As was the case for mean precipitation, also the extremes of LP mainly increase in winter (Figure 6). Thus winter precipitation is expected to increase not only in a mean sense but also in terms of short-term maxima. Concerning CP, a clear increase of the extremes is found during summer. The annual maximum local short-term precipitation extremes, for which for example storm runoff sewers are designed, are generally associated with convective summer rainfalls. The tendency in Figure 6 indicates that these rainfalls may significantly increase, which would thus have a distinct impact on urban hydrological design and management. It must however be emphasised that RCM-simulated summer precipitation extremes are associated with large uncertainties (e.g. Fowler and Ekström, 2009).

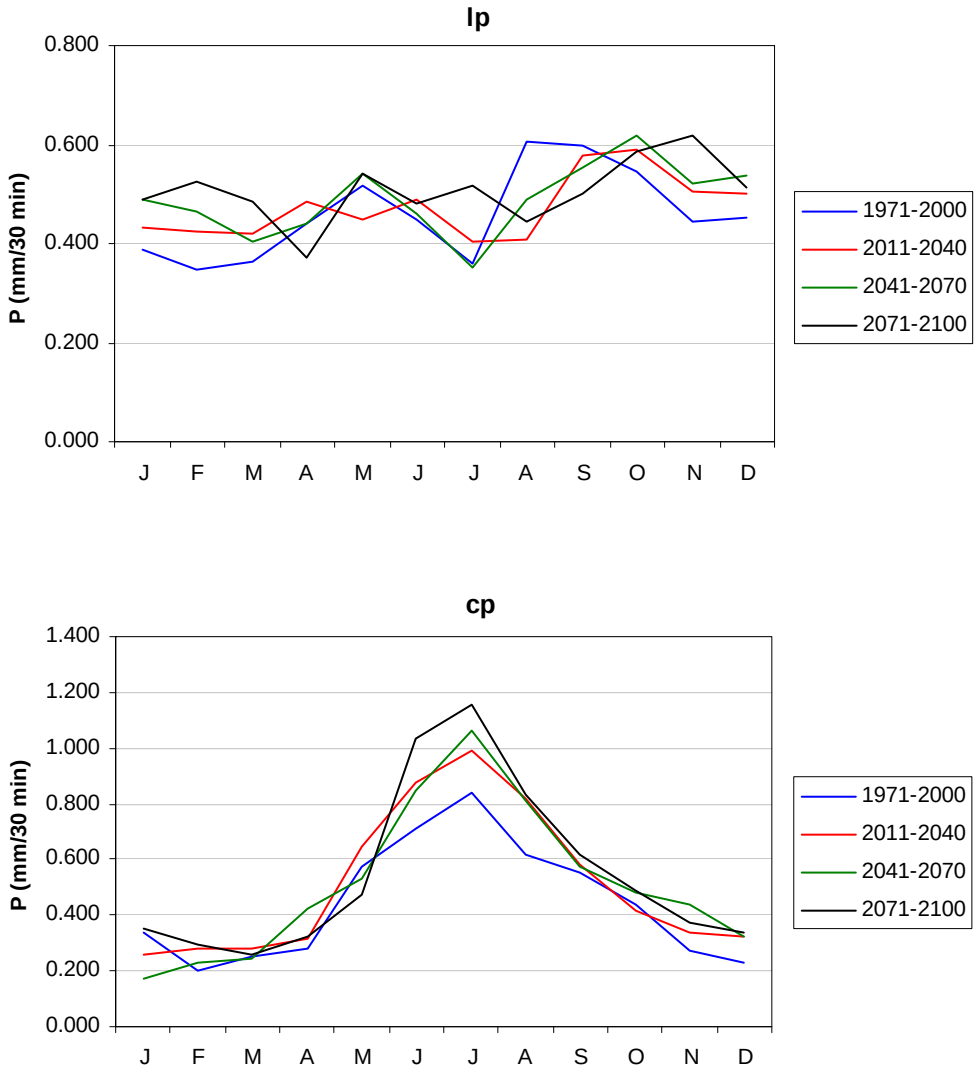

Figure 6 Monthly 97.5th percentile of large-scale (lp; top) and convective (cp; bottom) precipitation during the 30-year periods (scenario B2).

3.2. Cloud cover

In this section, cloud cover output from the RCA3 model with the ERA40-analysis at the boundaries is characterised. Comparison is made with satellite observations and future changes are investigated.

Cloud cover is expressed as the gridbox fraction (between 0 and 1) covered by clouds. Table 2 reveals that for total clouds (TC), this fraction is on average 0.64. As only very few (4%) of the 3-hr periods have a non-zero TC cover, the mean non-zero cover is similar. The high clouds (HC) cover on average 30% of the gridbox, and 43% when only non-zero periods are considered.

Table 2 Some descriptive statistics of cloud cover variables TC and HC in the RCA3/ERA40 simulation.

	Mean (-)	Percentage non-zero (%)	Mean non-zero (-)
RCA TC	0.64	95.9	0.67
RCA HC	0.30	70.2	0.43

In RCA3, the two types of cloud cover vary only slightly with season (Figure 7). Both TC and HC have their highest values in autumn. TC is lowest in spring and early summer, HC in mid-winter and mid-summer.

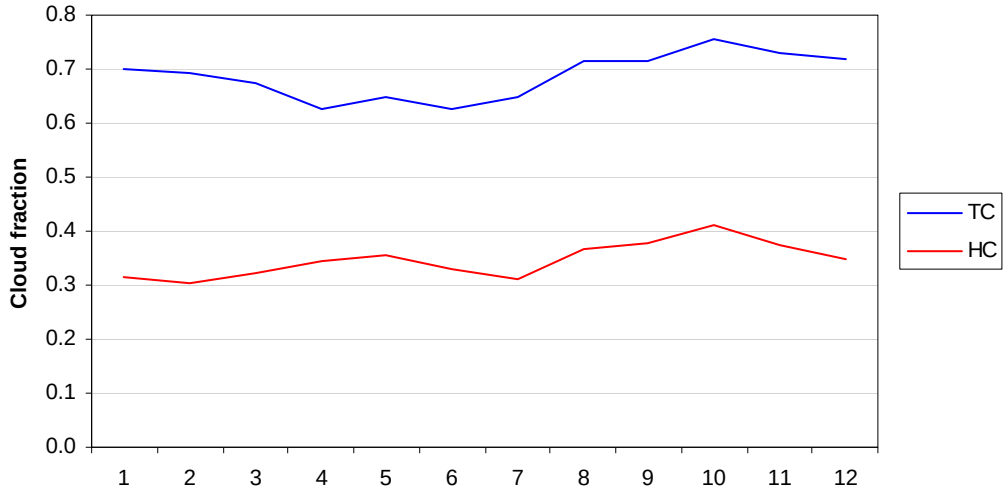

Figure 7 Monthly average fraction of total (TC) and high (HC) clouds in RCA3/ERA40.

An evaluation of the RCA3 cloud variables has been performed by Willén (2008) with a comparison with satellite observations. The analysis covered entire Europe, but for this report results have been extracted for the Stockholm region. The upper diagram in Figure 8 shows a comparison between simulated and observed cloud cover on a monthly basis in the period of 1997-2001. The simulated cloud cover overall reproduces very well the observed one. The lower diagram shows the simulated cloud cover separated into vertical categories (low, mid, high defined in section 2.2.2). As these may overlap, they have no clear relationship with the total cloud cover shown in the upper diagram.

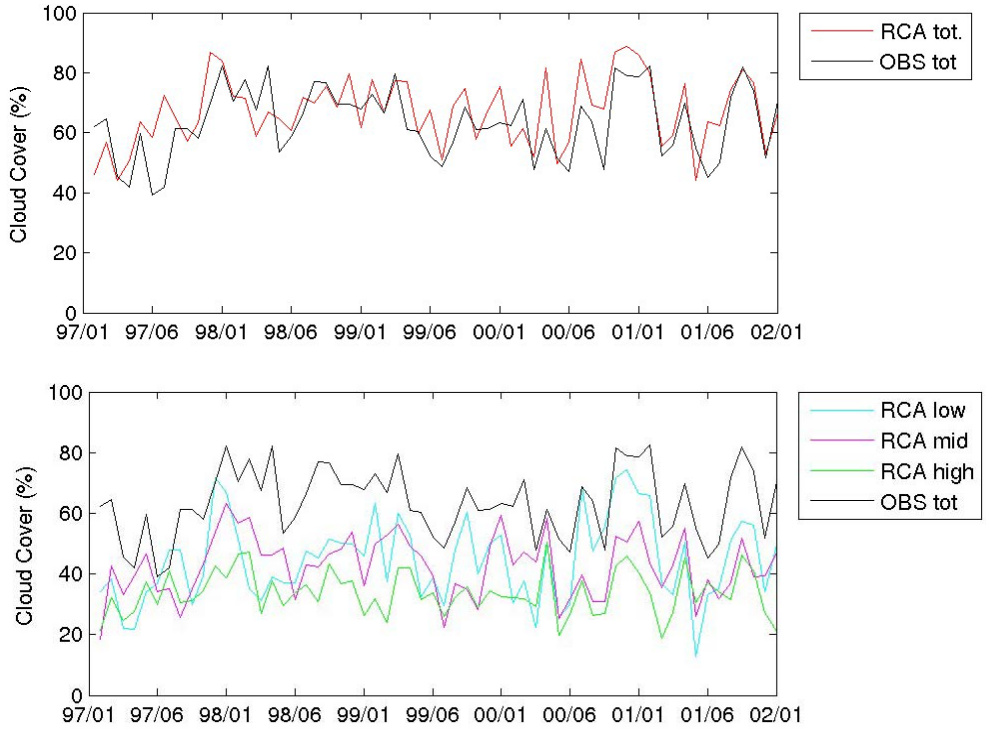

Figure 8 Monthly total cloud cover in Stockholm as observed (OBS) and as simulated by RCA3 (top). RCA3-simulated clouds divided into vertical categories (bottom).

Future changes in cloud cover as simulated in scenario B2 are very small (Figure 9). Neither TC nor HC shows any clear tendency to change compared with today's levels. Some assessment of the entire probability distributions was also made (not shown), but neither here was any significant future change apparent. The intra-annual variations in all future periods are nearly identical to the curves in Figure 7 representing today's climate.

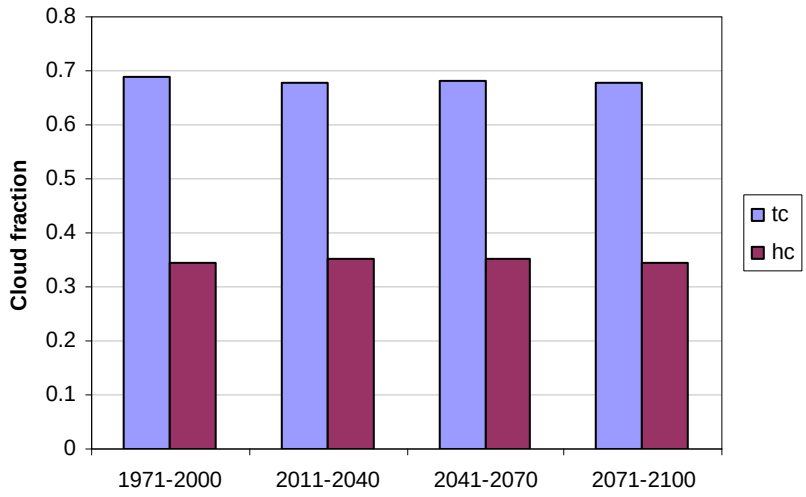

Figure 9 Mean cloud fractions during the 30-year periods (scenario B2).

4. Principal downscaling method

The principle of the suggested downscaling approach is shown in Figure 10. In the RCM output, total gridbox average precipitation P consists of one resolved (large-scale) component and/or one convective component, P_f and P_c in Figure 10 (P_f corresponds to LP above and P_c to CP). Each of these is assumed to be associated with a cloud cover fraction, C_f and C_c ($0 \leq C \leq 1$), respectively, represented by the white area in Figure 10. It is further assumed that the cloud cover fraction C is related to the fractional precipitation area A (shaded area) by a multiplicative parameter α, $0 < \alpha \leq 1$. Under these assumptions the actual local precipitation P_{point}, which occurs in a point located under the precipitation field, is given by P/A. If further assuming that the probability of precipitation is the same everywhere inside the gridbox, the probability of P_{point} occurring in an arbitrary point inside the gridbox equals the fractional precipitation area A.

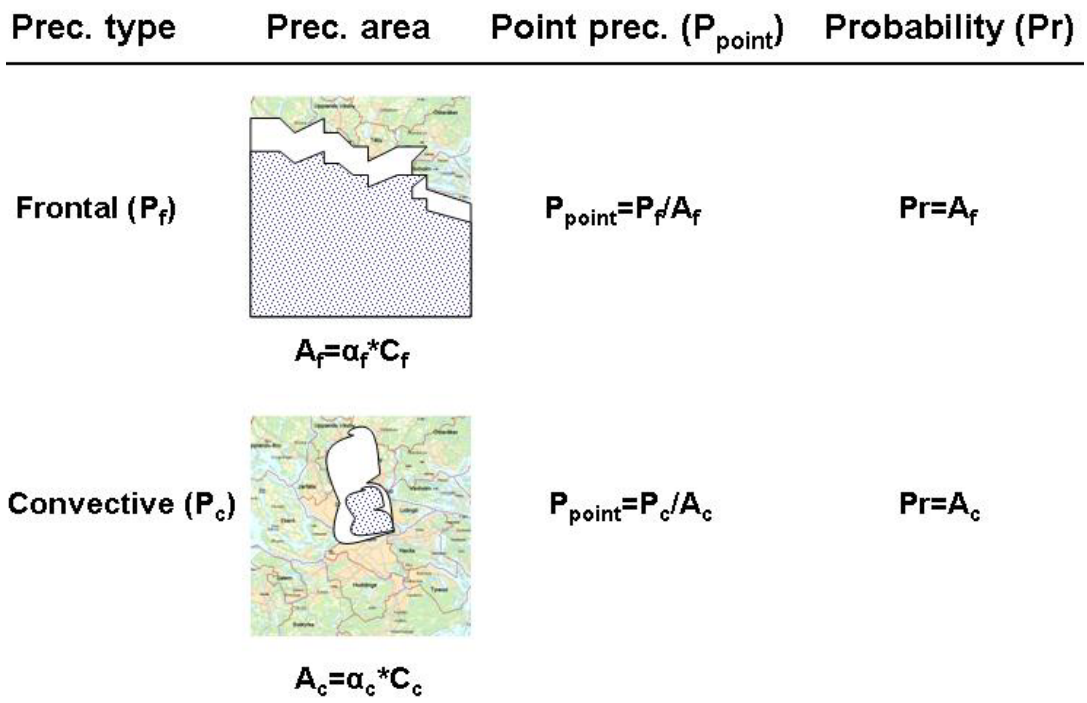

Figure 10 Schematic of the stochastic downscaling scheme.

Under these assumptions stated, a simplified scheme for stochastic simulation of precipitation time series in an arbitrarily located gauge may be developed. For each time step, first the gridbox average precipitation is rescaled to a local precipitation P_{point} based on the fractional cloud cover C and the associated precipitation area A. Second, a uniformly distributed random number r, $0 < r < 1$, is generated. If $r > A$ the precipitation field misses the gauge; if $r < A$ the precipitation field hits and the gauge registers P_{point}.

5. Approach 1: Total and high clouds

With respect to which cloud variables used to estimate the precipitation area A, two different approaches were used. In the first, the variables total clouds (TC) and high clouds (HC) were used. TC is used to represent C_f in Figure 10, i.e. the cloud cover related to frontal (resolved) precipitation, and HC is used to represent the cloud cover associated with convection C_c. In the second approach (Section 6), experimental analyses are performed using more elaborate cloud variables.

5.1. Evaluation for historical RCA3 simulation (ERA40)

As the precipitation downscaling scheme is stochastic, each time it is applied to the same gridbox time series a different point time series realisation is generated. The downscaling results presented in the following represent averages over 100 realisations, which was found sufficient for obtaining stable estimates. As this study is focused on extreme point precipitation, the evaluation is made mainly in terms of IDF-curves and precipitation amounts related to long return periods.

Downscaling using the principal method described in the previous section was attempted both with and without tuning the estimation of the rainfall area A based on the cloud cover C. No tuning implies that the multiplicative parameter $\alpha=1$, i.e. the precipitation area A equals the cloud cover C.

5.1.1. Downscaling without tuning

Especially for the shortest durations, the IDF-curves of downscaled point precipitation are substantially closer to the observed curves than the IDF-curves produced from RCA3 gridbox data (Figure 11). The observed values are however still notably higher, i.e. the downscaled extreme intensities are underestimated. At long durations the downscaling has no effect. This is probably due to that these extremes are generated by large-scale synoptic systems with cloud covers C equal or close to 1, i.e. point precipitation becomes equal or close to the gridbox average precipitation.

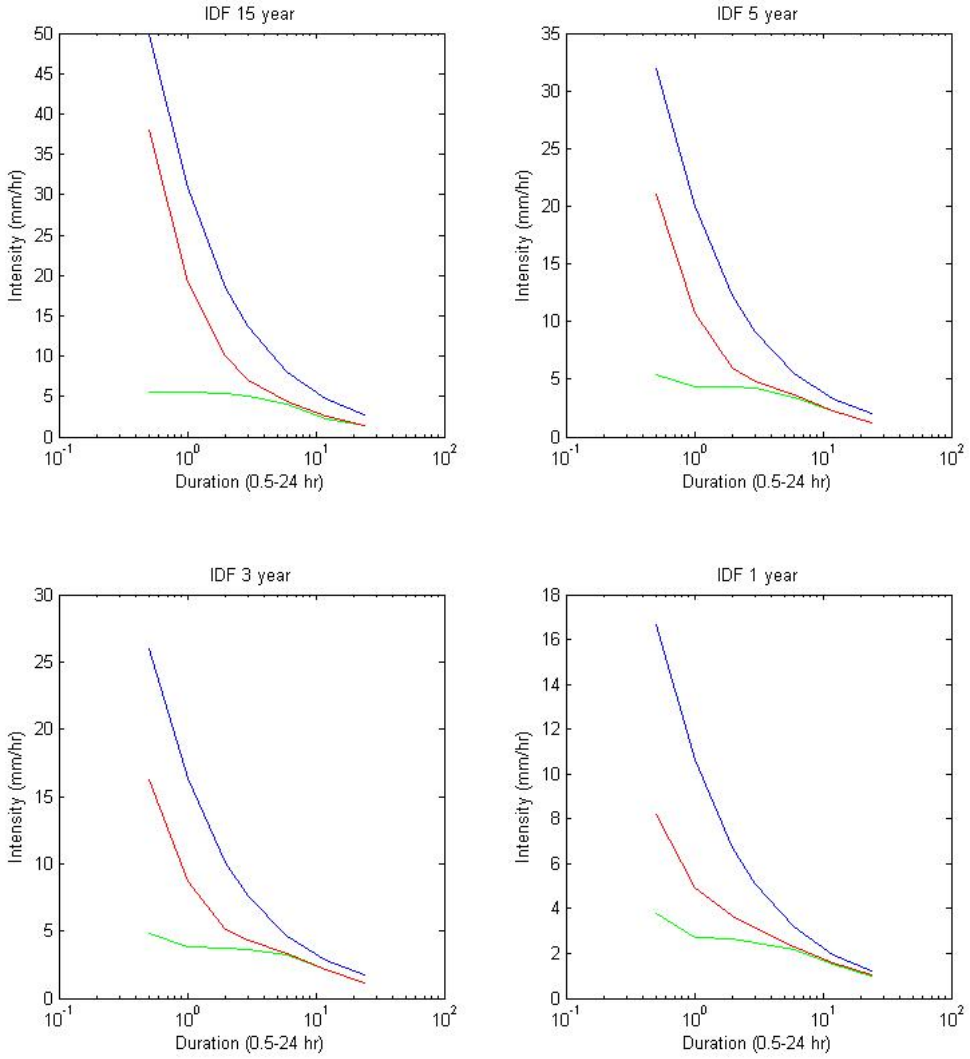

Figure 11 IDF curves representing TB observations (blue), RCA3/ERA40 gridbox output (green) and point simulations by untuned downscaling (red) for return periods 15, 5, 3 and 1 year.

5.1.2. Downscaling with tuning

From the evaluation of RCA3 precipitation and clouds in Chapter 3 it could be suspected that untuned downscaling would not generate high enough extreme short-term point precipitation intensities. As discussed in connection with Table 1 and Figure 2, short-term point extremes are up to 10 (5 if the single highest value is excluded) times higher than the RCA3 gridbox extremes. To generate such point extremes, the gridbox precipitation thus needs to be concentrated into 1/10 of the gridbox, i.e. A=0.1. But as shown in Table 2 the cloud cover, C, which equals A in untuned downscaling, is typically rather 0.4-0.7.

Attempts to improve the agreement between observed and downscaled IDF-curves were made by calibration of the α-parameter to an optimal value below 1. This means that the generated rainfall field is smaller than the cloud cover, which is physically reasonable.

For the RCA3/ERA40-simulation, an α_c-value of ~0.12 was found optimal. In some cases, however, when HC is small, this makes A_c very small and then P_{point} may become unrealistically high. Therefore a minimum HC-threshold was used. A value ~0.1 (i.e. 10% fractional cover) was found suitable. With a grid size of 50×50 km and an α_c-value of 0.12, a threshold of 0.1 implies that 30 km² would be a lower limit of the spatial extension of the 30-min areal rainfall generated by convective precipitation. Further work will aim at studying this value on theoretical and/or empirical grounds.

Concerning frontal precipitation, instead of reducing the area of TC by the parameter α_f, it was found more suitable to use a cut-off limit for the large-scale precipitation component P_f. This is also done in other hydrological applications of the RCA3 (and other GCM/RCM) data, to remove excessive and possibly spurious low precipitation. In this application a threshold of ~0.15 mm was found optimal. It may be noted that the treatment of large-scale precipitation has only a minor impact on the simulated IDF-curves which are governed by convective precipitation.

Figure 12 shows that it is possible to reproduce the observed IDF-curves with an acceptable accuracy by tuned downscaling. The main difference between the observed and downscaled curves is a somewhat higher degree of curvature in the simulated curves, i.e. the rate of increase in extreme intensity with decreasing duration is somewhat overestimated. However, it does not seem possible to significantly change the curvature by the present simple formulation of the downscaling scheme.

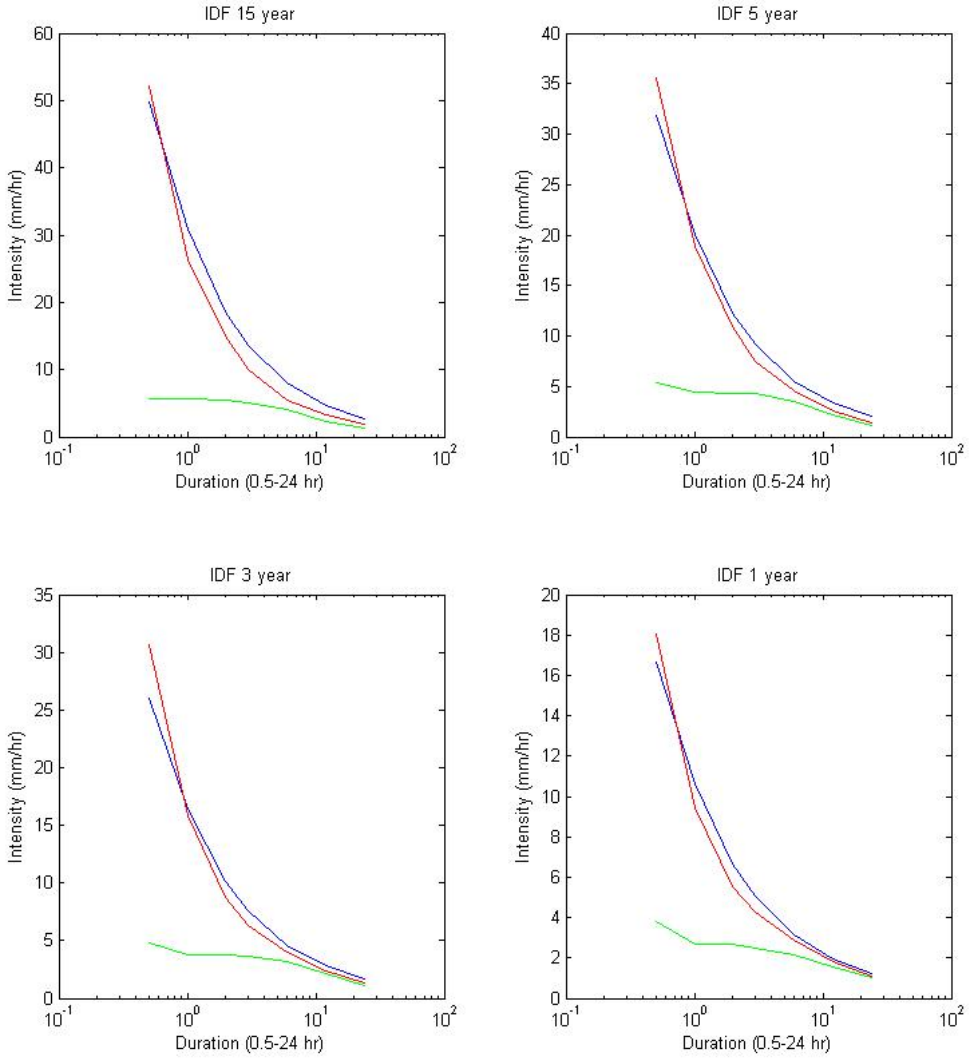

Figure 12 IDF curves representing TB observations (blue), RCA3/ERA40 gridbox output (green) and point simulations by tuned downscaling (red) for return periods 15, 5, 3 and 1 year.

Concerning the intra-annual variation of extremes and high values, this is overall similar to the original RCA3/ERA40 data, as shown in Figure 13 (compare with Figure 3). For the downscaled data, however, high values are generally mainly related to convection. This occurs in ~80% of the cases. The events containing the maximum intensities last on average ~2.5 hours, which is close to the value of 3 hours found for the observations.

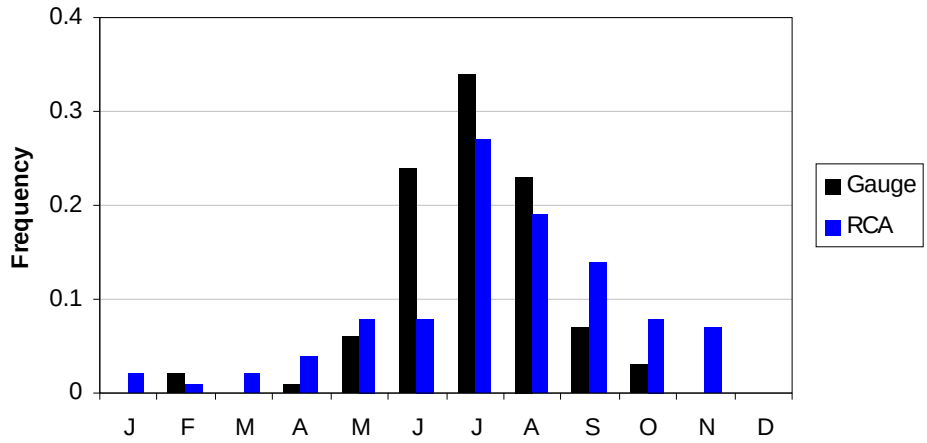

Figure 13 Intra-annual variation of extremes in the TB observations (gauge) and point simulations by tuned downscaling (RCA).

5.2. Application to future climate projections

In this section the stochastic downscaling scheme is applied to the A2, B2 and A1B scenarios. Both untuned and tuned downscaling was performed. In the latter the parameters were optimised using scenario data in the REF period 1971-2000 (the same parameter values were used for all scenarios). The resulting parameter values were overall similar to the ones obtained in the optimisation to RCA3/ERA40 data (Section 5.1.2).

The resulting 10-year IDF-curves indicate a future increase in the short-term point precipitation extremes (Figure 14). In the B2 scenario most of the increase happens between REF and FC1, with rather minor additional increase until FP3. In the A1B scenario, however, most of the increase happens between FC1 and FC2, and in A2 the increase from REF to FC3 is gradual (not shown).

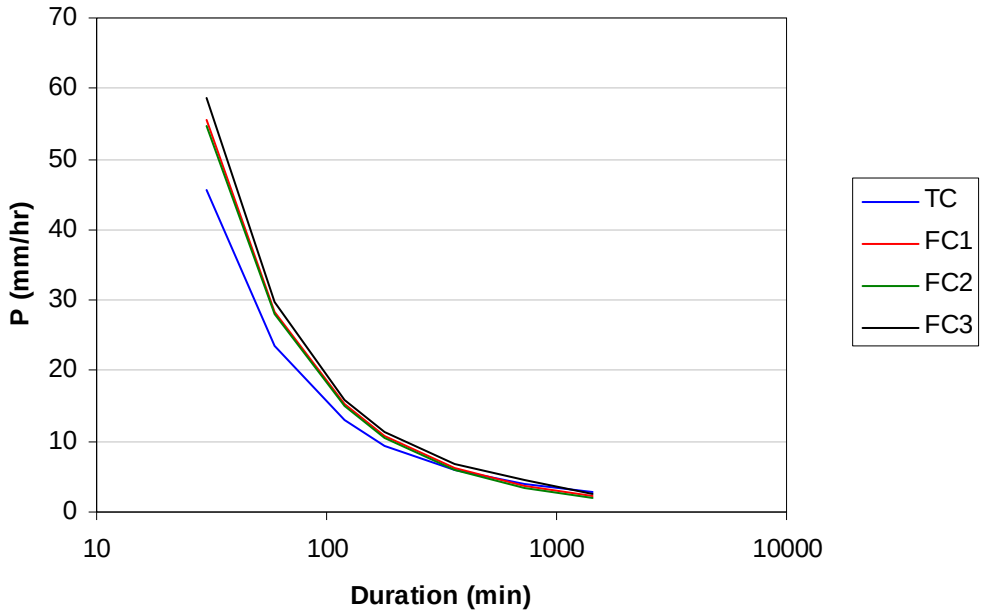

Figure 14 10-year IDF-curves for the 30-year periods (TC=REF=1971-2000) estimated by tuned downscaling (scenario B2).

Examples of relative changes in 10-year precipitation intensity of different durations, i.e. effectively the ratios of future to present IDF-curves, are shown in Figure 15. Looking at FC1, there is a substantial variation between the scenarios. In B2 the short-duration extremes increase by some 20% whereas the long-duration extremes decrease by almost the same amount. This implies an increased intensity of localised, convective rainfalls, but a decreased intensity of precipitation associated with large-scale synoptic systems. In A1B the picture is almost the opposite, with a small decrease of short-duration extremes and a 20-30% increase of the long-duration extremes. The change found in scenario A2 is in between the others. On average over all scenarios the change ranges from 10% for duration 30 min to 3% for duration 1 day.

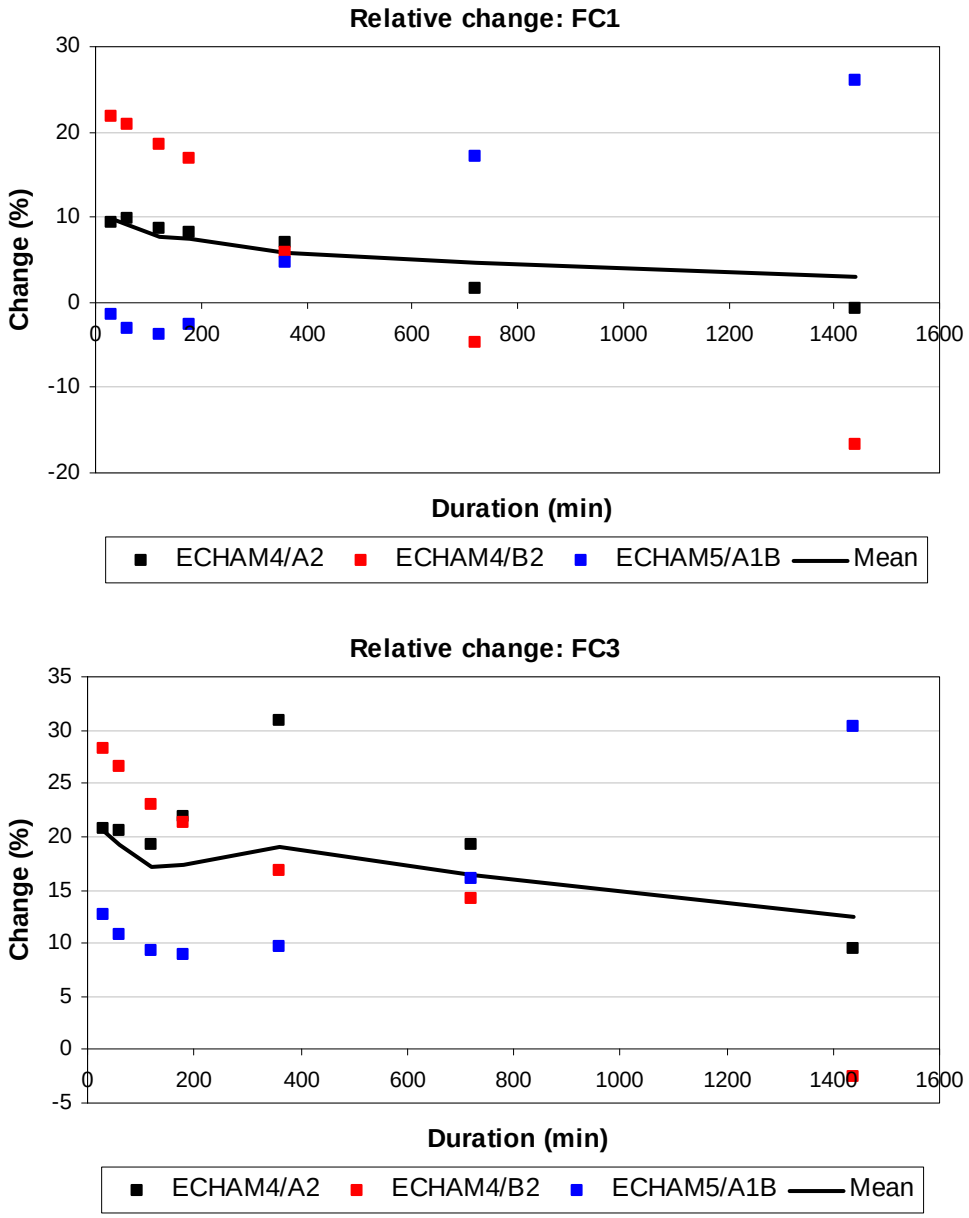

Figure 15 Relative change in 10-year precipitation intensity estimated by tuned downscaling. The solid line represents average change.

It was attempted to interpret the opposite tendencies found in the B2 and A1B scenarios in light of the characterisation of future precipitation in Section 3.1.2. Figure 6 implies a rather pronounced increase in convective extremes between REF and FC1 for scenario B2, in line with the estimated change in Figure 15. Concerning extreme large-scale precipitation, the annual maximum is higher in REF than in FC1 (Figure 6), which also supports the changes found. An evaluation of scenario A1B is however less clear-cut. Also in A1B convective extremes do increase, in contrast with Figure 15, although the increase is less pronounced than in B2. In A1B the large-scale maximum is slightly higher for FC1 than for REF, but far from the 20-30% indicated in Figure 15. It must be emphasised that the extreme statistics are governed by the precipitation occurring on a few short periods. Thus, there might not be any clear links to more general changes.

The changes obtained for period FC3 vary similarly to the ones found for FC1, but are consistently shifted upwards by some 10%. The average change ranges from 20% for 30 min to 13% for 1 day.

The changes estimated from stochastic untuned downscaling (Figure 16) are overall similar to the ones from tuned downscaling, with similar trends in the scenarios and similar levels of the average changes. One difference is that the rather clear tendency of a larger increase for shorter durations found is not evident in the untuned downscaling. A possible explanation is that the future increase of short-term convective extremes becomes accentuated in the tuned downscaling, because of its stronger concentration of gridbox precipitation into smaller areas.

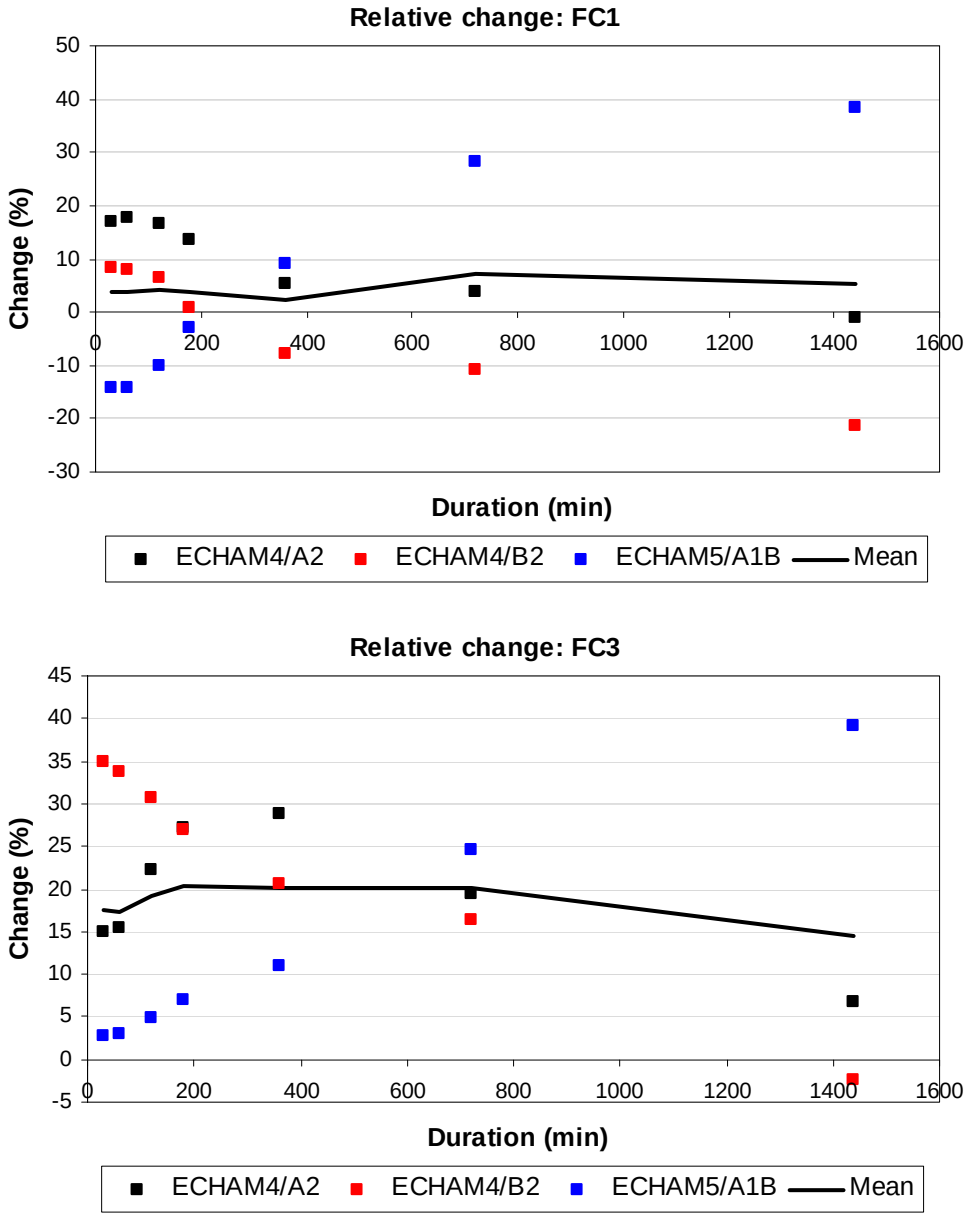

Figure 16 Relative change in 10-year precipitation intensity estimated by untuned downscaling. The solid line represents average change.

Finally, in Figure 17, the future changes in short-term point precipitation extremes estimated using downscaled time series are compared with the changes estimated directly from RCA3 gridbox average precipitation time series. For FC1, a small average decrease by 4% of the short-term extremes at the gridbox scale is suggested. As the changes in individual scenarios vary widely by ±20% over the entire range of scenarios, effectively no difference from REF is found. For FC3, the average gridbox scale change ranges from 15% for 30 min to 8% for 1 day. In this case there is much less variation between the scenarios but they are all rather close to the average curve in Figure 17.

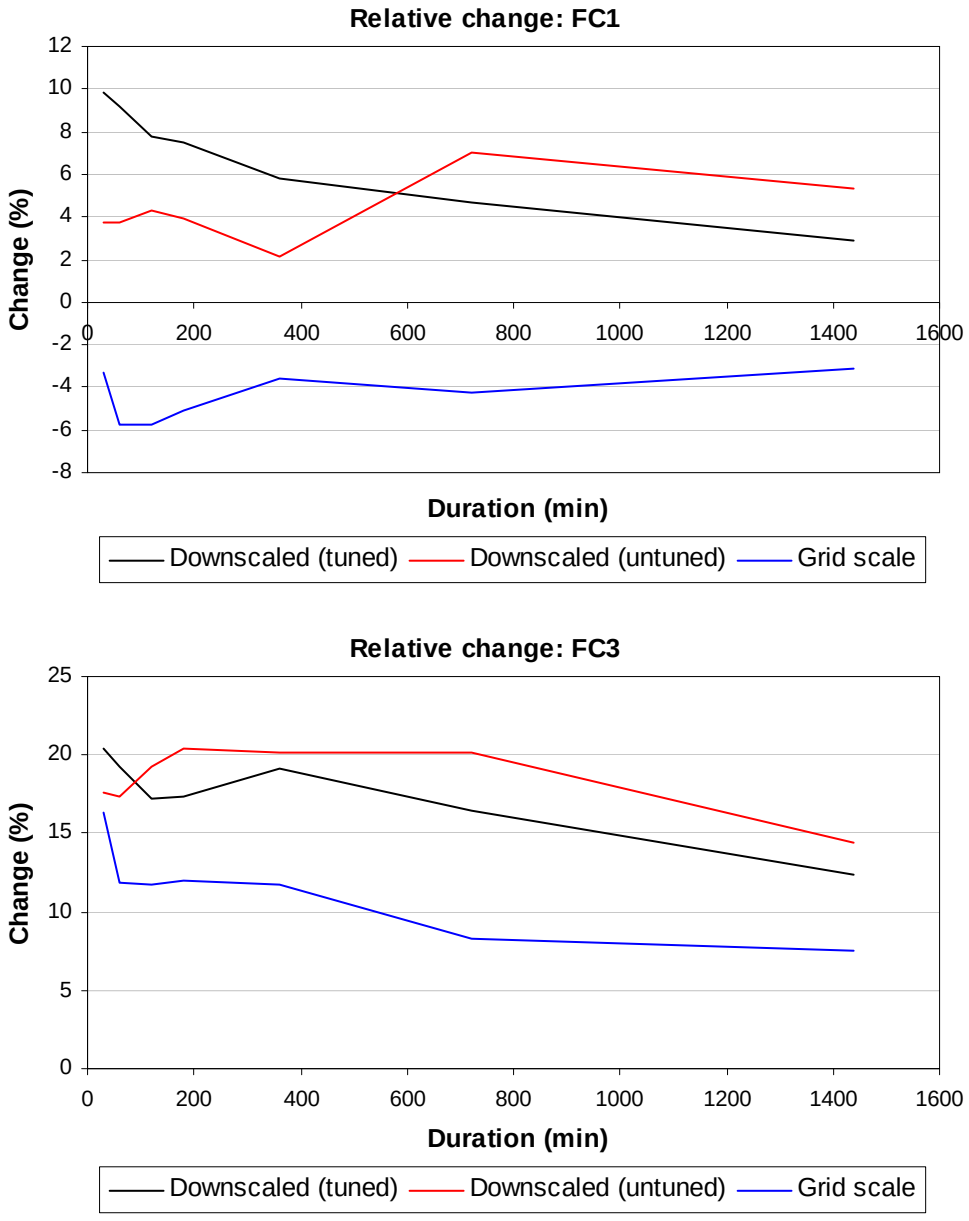

Figure 17 Relative change in 10-year precipitation intensity estimated by tuned downscaling, untuned downscaling and at the gridbox scale. The curves represent averages over the three scenarios used.

The relative increase estimated from downscaled series is consistently 5-10% larger than that estimated from gridbox series. This may indicate that the future increase in local short-term point precipitation extremes, which are mainly related to convective events, becomes larger than the short-term increase estimated from 50-km RCA3 gridbox average precipitation, which is mainly related to large-scale events. It must however be emphasised that the application of the stochastic downscaling scheme to the original RCA3 gridbox data introduces a substantial amount of uncertainty. Thus, while supposedly better representing local precipitation, the changes estimated from downscaled series are clearly less robust than the changes at gridbox scale. A practical approach may be to view the gridbox-scale changes as conservative estimates of changes also on smaller scales.

6. Approach 2: Detailed cloud variables

In this final section, an additional set of more detailed cloud variables are evaluated with respect to their applicability in the downscaling scheme. These variables are only available for the RCA3/ERA40-simulation. Thus, no analysis of future climate is possible. The variables are:

- Total Cloud cover, maximum-Random overlap TCR
- Large-scale Cloud cover, maximum-Random overlap LCR (time step: 30 min)
- Convective Cloud cover, maximum-Random overlap CCR
- Total Cloud cover, Maximum overlap TCM
- Large-scale Cloud cover, Maximum overlap LCM (time step: 30 min)
- Convective Cloud cover, Maximum overlap CCM
- Convective radius, CRAD, TC (3 hr)

TCR is the same as TC earlier in this report and it is a sum of all the three cloud types in RCA3: convective, shallow convective and large scale, at each model level, the total cloud cover at the surface calculated using the standard maximum-random overlap. We also calculate the cloud cover at the surface for all the individual cloud types using both the maximum-random overlap and using pure maximum overlap. For the maximum overlap assumption we assume all cloud fractions are vertically stacked in the grid column, which is the same as choosing the largest fraction in the vertical as representative for the whole grid column. We added all these variables to the model output at each time step in order to identify the most appropriate cloud cover to be used in the downscaling.

Characteristics of the additional cloud variables are given in Table 3. TCR is identical to the variable TC used previously, and the properties of LCR is nearly identical to TCR, since the CCR clouds rarely occur they will not contribute much to the mean total cloud cover. The convective variable CCR is zero some 95% of the time, but when it is not the cloud fraction is on average 0.61. The properties of maximum overlap variables are nearly identical to their corresponding random overlap variables, indicating there are few vertical levels with zero cloud fraction (the cloud fraction will be in maximum overlap). The non-zero average CRAD value 728 m implies a cloud area of 1.7 km², i.e. a fractional cloud cover of 1.7/2500=0.0007.

Table 3 Descriptive statistics of the additional cloud variables in the RCA3/ERA40 simulation.

	Mean (-)	Non-zero percentage (%)	Mean non-zero (-)
TCR	0.64	96.0	0.67
LCR	0.64	96.0	0.66
CCR	0.02	2.7	0.61
TCM	0.60	95.9	0.62
LCM	0.59	95.9	0.61
CCM	0.02	2.7	0.58
CRAD	279 m	38.4	728 m

The cloud variables were tested in untuned downscaling as outlined in Chapters 4 and 5, by using TCR (TCM) or LCR (LCM) to estimate C_f and CCR (CCM) or SCR (SCM) or CRAD to estimate C_c. No improvement was however found compared with using TC and HC. The best result was found using LCR (or LCM) and CCR (or CCM) (Figure 18; note that the y-axis is logarithmic). The downscaled IDF-curves are closer to the observed one than the gridbox curves, but the extreme intensities for long durations increase too much and for short durations too little. When using CRAD instead of CCR (CCM) the extreme intensities become overestimated by up to 10 times and even more, which is a result of the very small fractional cloud covers associated with CRAD.

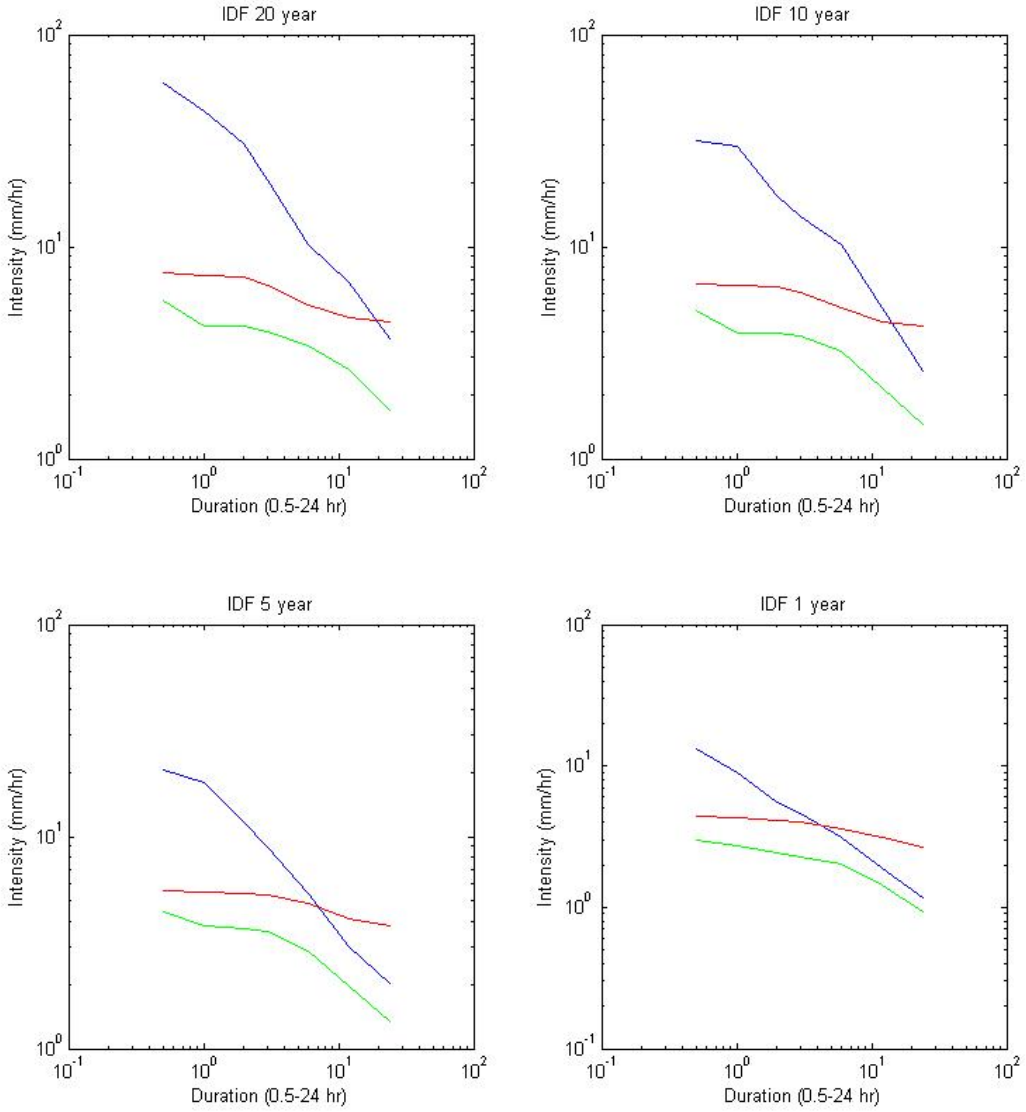

Figure 18 IDF curves representing TB observations (blue), RCA3/ERA40 gridbox output (green) and point simulations by untuned downscaling by LCR and CCR (red) for return periods 20, 10, 5 and 1 year.

This first assessment of the detailed cloud variables does not indicate any improvement. It is possible that a better performance could have been reached by tuned downscaling, but that has not been tested in this study. More work is required to understand how the different cloud variables function in the downscaling scheme and which variables are most sensible from a physical point of view.

7. Conclusions

Some key conclusions from this study are in the following:

- The annual cycle of mean monthly total precipitation from RCA3 agrees well with observations, although a slight overestimation is found. The frequency is however overestimated, especially of large-scale (resolved) precipitation. Also the mean monthly RCA3 cloud cover agrees well with observations.

- No clear future change in the cloud cover was found. Large-scale and convective precipitation both increase gradually by some 20% by the period of 2071-2100. Total and large-scale precipitation extremes increase mainly in winter; convective extremes in summer.

- After tuning, a simple stochastic downscaling scheme based on precipitation type and cloud cover can simulate point precipitation time series which satisfactorily reproduce observed extreme statistics.

- The downscaled series indicate a 5-10% increase in short-term extreme intensities in period 2011-2040 and a 10-20% increase in period 2071-2100. This is 5-10% more than what is estimated from RCA3 gridbox data.

- Using more detailed cloud variables than 'total clouds' and 'high clouds' did not improve performance of the downscaling scheme.

The main finding is the indication of a larger increase in short-term extreme precipitation on the point scale than on the RCA3 gridbox scale. Thus the future increase of local precipitation intensities may become larger than what can be inferred from climate model output. However, the point scale results consider less robust than the gridbox scale results and thus the results must be interpreted with caution.

It must be emphasised that the suggested downscaling scheme is mainly intended as a prototype. For example, temporal correlation is missing, i.e., the adjacent time steps are independent, which makes the autocorrelation in downscaled point time series lower than in observed series. Otherwise, despite its simplicity, the scheme appears to be able to surprisingly well reproduce not only extreme statistics but also most relevant mean statistical properties such as annual total, wet fraction and the volume and duration of individual precipitation events.

It must also be emphasised that this is a case study for a specific location, specific climate models and a set of three future emission scenarios. To assess the general applicability of the approach, further testing in other locations using other models and scenarios are ongoing. A key issue is the current rapid increase in the spatial resolution of RCMs. Comparison with high-resolution short-term RCM-precipitation will indicate whether statistical downscaling is soon redundant.

References

Bony S., and Emanuel, K.A., 2001. A parameterization of the cloudiness associated with cumulus convection; Evaluation using TOGA COARE data. *J. Atmos. Sci.*, 58, 3158–3183.

Brown, J.M., 1979. Mesoscale unsaturated downdrafts driven by rainfall evaporation. *J. Atmos.Sci.*, 36, 313-38.

Fowler, H. J., and Ekström, M., 2009. Multi-model ensemble estimates of climate change impacts on UK seasonal precipitation extremes. *Int. J. Climatol.*, 29(3), 385-416.

Haylock, M.R., Hofstra, N., Klein Tank, A.M.G., Klok, E.J., Jones, P.D. and New, M., 2008. A European daily high-resolution gridded data set of surface temperature and precipitation for 1950-2006. *J. Geophys. Res.*, 113, D20119, doi:10.1029/2008JD010201.

Hernebring, C., 2006. *10-års regnets återkomst förr och nu (Design storms in Sweden then and now)*. VA-forsk publ. 2006-04, Svenskt Vatten, Stockholm (in Swedish).

Jones, C.G., Ullerstig, A., Willén, U. and Hansson, U., 2004. The Rossby Centre regional atmospheric climate model (RCA). Part I: Model climatology and performance characteristics for present climate over Europe. *Ambio*, 33(4-5), 199-210.

Kain, J.S. and Fritsch, J.M., 1990. A one-dimensional entraining/detraining plume model and its application in convective parameterization, *J. Atmos. Sci.*, 47, 2784-2802.

Kjellström, E, Bärring, L., Gollvik, S., Hansson, U., Jones, C., Samuelsson, P., Rummukainen, M., Ullerstig, A., Willén, U. and Wyser, K., 2005. *A 140-year simulation of the European climate with the new version of the Rossby Centre regional atmospheric climate model (RCA3)*. Reports Meteorology and Climatology 108, Swedish Meteorological and Hydrological Institute, SE-601 76 Norrköping, Sweden.

NERC, 1975. *Flood Studies Report*. Volumes I–V. National Environmental Research Council, London, UK.

Olsson, J., Berggren, K., Olofsson, M., and Viklander, M., 2009. Applying climate model precipitation scenarios for urban hydrological assessment: a case study in Kalmar City, Sweden. *Atmos. Res.*, 92, 364-375.

Rasch, P.J., and Kristjánsson, J.E., 1998. A comparison of the CCM3 model climate using diagnosed and predicted condensate parameterizations. *J. Climate*, 11, 1587–1614.

Slingo, J., 1987. The development and verification of a cloud prediction scheme for the ECMWF model. *Quart. J. Roy. Meteor. Soc.*, 113, 899-928.

Sundqvist, H., E. Berge and Kristjansson, J.E., 1988. Condensation and cloud parameterisation studies with a mesoscale numerical weather prediction model. *Mon. Wea. Rev.*, 117, 1641-1657.

Willén, U., Crewell, S., Baltink, H. K. and Sievers, O. 2005. Assessing model predicted vertical cloud structure and cloud overlap with radar and lidar ceilometer observations for the Baltex Bridge Campaign of CLIWA-NET. *Atmos. Res.* 75:3, 227-255, doi:10.1016/j.atmosres.2004.12.008.

Willén U., 2008. *Preliminary use of CM-SAF cloud and radiation products for evaluation of regional climate simulations*. Reports Meteorology 131, Swedish Meteorological and Hydrological Institute, SE-601 76 Norrköping, Sweden.

Xu, K.-M. and Krueger, S., 1991. Evaluation of cloudiness parameterisations using a cumulus ensemble model. *Mon. Wea. Rev.*, 119, 342-367

Mistra SWEdish research programme on **C**limate, **I**mpacts and **A**daptation is a research programme on advanced analysis and consistent assessment of climate, economy, impacts and adaptation.

See www.mistra-swecia.se for up-to-date information about the programme.

The programme is funded by Mistra, the Foundation for Strategic Environmental Research (see www.mistra.org). The main research partners are the SMHI, the Department of Physical Geography and Ecosystems Analysis at Lund University, the Department of Meteorology and the Institute for International Economic Studies at Stockholm University, and the Stockholm Environment Institute. The SMHI is also the programme management organisation.

SMHI, SE-601 76 Norrköping, Sweden
info@mistra-swecia.se, www.mistra-swecia.se